IEEE Open Journal of
Industry Applications

Received 22 November 2023; revised 11 March 2024 and 25 April 2024; accepted 7 May 2024. Date of publication 9 May 2024;
date of current version 21 May 2024. The review of this article was arranged by Associate Editor L. Solero.

Digital Object Identifier 10.1109/OJIA.2024.3399009

Robust Control of Synchronous Reluctance Motor Based on Automatic Disturbance Rejection

ANGELO ACCETTA [1] (Senior Member, IEEE), MAURIZIO CIRRINCIONE [2] (Senior Member, IEEE), FILIPPO D'IPPOLITO [3] (Senior Member, IEEE), MARCELLO PUCCI [1] (Senior Member, IEEE), AND ANTONINO SFERLAZZA [3] (Senior Member, IEEE)

[1]Institute for Marine engineering, section of Palermo, National Research Council of Italy, 90146 Palermo, Italy
[2]School of Engineering and Physics, University of the South Pacific, Suva 0679, Fiji
[3]Department of Engineering, University of Palermo, 90128 Palermo, Italy

CORRESPONDING AUTHOR: MARCELLO PUCCI (e-mail: marcello.pucci@cnr.it)

This work was supported by the USP-SRT Research Project: Advanced Control of Synchronous Reluctance Motors for Electrical Vehicles (ACOSREV) .

ABSTRACT This article proposes the theoretical development and experimental application of the active disturbance rejection control (ADRC) to synchronous reluctance motor (SynRM) drives. The ADRC is a robust adaptive extension of the input-output feedback linearization control (FLC). It performs the exact linearization of the SynRM model by a suitable nonlinear transformation of the state based on the online estimation of the corrective term by the so-called extended state observers (ESO). Consequently, any unmodeled dynamics or uncertainty of the parameters are properly addressed. The control strategy has been verified successfully both in numerical simulations and experimentally on a suitably developed test set-up that provides the ADRC robustness versus parameters variations which cannot be obtained with other model-based nonlinear control techniques (e.g., FLC). Simulation results show the capability of the ADRC to maintain its dynamic performance, even in the presence of quick variations of the SynRM dynamic inductances. Experimental results confirm the robustness of the ADRC versus any model parameter uncertainty. The proposed ADRC has been experimentally compared with a previously developed FLC, in both a tuned and detuned working configuration, with the classic rotor oriented control, and with a finite state model predictive control (MPC), where speed control is integrated into the MPC. Experimental results show far better robustness versus any parameter variation.

INDEX TERMS Synchronous reluctance motor (SynRM), active disturbance rejection control (ADRC), feedback linearization control (FLC), extended state observer (ESO), saturation effects.

I. INTRODUCTION

Nowadays, synchronous reluctance motors (SynRMs) have seen an ever-increasing boost in several industry applications requiring accurate torque and speed control with high efficiency in the whole speed range, even at partial load.

In general, the control of SynRM is very challenging, given that its theoretical performance is limited by the strong nonlinearity of the machine, particularly because of its magnetic characteristics. Actually, saturation phenomena are different on the direct and quadrature axes, and significant cross-saturation phenomena are observable. As far as vector control strategies of SynRMs are concerned, several kinds of orientations have been conceived, among which the classic orientation on the rotor minimum reluctance axis (ROC = Rotor oriented control), on the stator flux (FOC = Field oriented control) or on the so-called active flux (A-FOC) [1], [2], [3], [4]. The SynRM drive is usually operated under maximum torque per ampere (MTPA) working condition. Its flux level is online modified according to the load torque. This can be achieved, in ROC by varying the amplitude of the direct stator current component, in FOC by varying the amplitude of stator flux amplitude, and, finally, in A-FOC by varying the

amplitude of the so-called active flux. However, in variable flux working conditions (e.g., under MTPA), whatever the field on which the orientation is performed, the speed and the flux control loops remain coupled by the torque equation ([5]), with a consequent unavoidable worsening of the SynRM drive dynamic performance. One way to decouple the speed and flux loops under variable flux conditions is to adopt suitable nonlinear control techniques, in particular, the so-called input–output feedback linearization control (FLC). FLC has been initially used with specific regard to induction motor (IM) drives [5], [6]. Nevertheless, very few applications of FLC to SynRMs are present in scientific literature so far [7], [8], [9], [10]. Recently, Accetta et al. [11] proposed an FLC for SynRM drives based on a particularly accurate dynamic model of the SynRM accounting for both self and cross-saturation and the mechanical equation of the drive, and thus, inherently permits the flux and speed loops to be properly decoupled in variable flux working conditions.

However, the input–output FLC technique is a model-based control and, therefore, suffers primarily from two disadvantages: 1) the accuracy of the dynamic model on which the control law is based; and 2) the corresponding correct knowledge of the model parameters.

ADRC [12], [13], [14] represents one effective solution to the above-cited limits of the FLC since it does not require the a priori knowledge of a model to perform the nonlinear transformation of the state. Unlike the FLC approach, the estimation of this function is generally carried out online, and a disturbance observer can be adopted. In this respect, the extended state observer (ESO) is a possible choice. Synthetizing, ADRC provides plant control robustness versus model uncertainty and parameter variations, still maintaining the best dynamic performance achievable by the SynRM. This is the main advantage of the proposed ADRC over other high-performance control techniques present in scientific literature.

In the field of synchronous motor drives, ADRC has been applied several times to control permanent magnet synchronous motors (PMSM): [15], [16], [17], [18], [19], [20], [21]. In particular, the authors [15] and [16] proposed the canonical ADRC applied to PMSM while the other works proposed slightly different versions with some peculiarities, for example, the authors in [17] dealt with a novel parallel structure to improve dynamic responses, which replaces the traditional cascade structure of position and speed loops. Qu et al. [18] proposed an enhanced linear active disturbance rejection controller (ADRC)-based rotor position sensorless field-oriented control scheme. Lin et al. [19] investigated a class of linear–nonlinear switching ADRC to design speed controllers and current controllers for PMSM in servo systems, which aims at enhancing the ability of disturbance rejection of speed and current controllers. Tian et al. [20] dealt with the performance deterioration due to dc and ac disturbances, and it proposes a discrete-time repetitive control-based ADRC for the current loop. Finally, Zhang [21] proposed a linear ADRC with a variable gain load torque sliding mode observer to reduce the effects of the load torque disturbance of interior PMSMs. Recently, the authors in [22] and [23] proposed ADRC approaches. In particular, Diab et al. [22] proposed an enhanced linear ADRC (ELADRC)-based rotor position sensorless field-oriented control scheme for the permanent magnet synchronous motor (PMSM) drives. In [22], the ADRC approach is used for current control, so from this point of view, it is hardly comparable to the proposed paper. Hou et al. [23] proposed a nonlinear ADRC for PMSM speed controller with frequency domain analysis. A nonlinear ESO (NESO) using a finite-time technique is constructed to enhance the antidisturbance property. On this basis, the NESO with a small bandwidth is sufficient to guarantee strong robustness without sacrificing noise suppression performance.

Although there are all these examples PMSM, there are not applications of ADRC to SynRM to the best of the authors' knowledge. From this standpoint, this article proposes an original theoretical approach by applying the ADRC to SynRM drives, which is most useful for those applications that need a good rejection against speed and load torque perturbations. It should be noted that the application of the ADRC to SynRM reveals, in the authors' opinion, more challenging than in the classic PMSM case, both interior mounted and surface mounted. The reason is that, in the SynRM case, both the static and dynamic inductances on the direct and quadrature axis are highly different (because of the desired saliency), and, more problematic, they are strongly varying with both the direct and quadrature components of the stator currents. This feature makes the application of ADRC on SynRM drives more challenging than in the other PMSM cases, given that the compensation terms estimated by the esos are highly varying with the operating conditions. This is one of the original aspects of the proposed approach. This article can be considered a follow-up and upgrade of [11], in the sense that with the proposed approach, no accurate analytical model is required because the nonlinear functions to linearize the system are computed online. In this article, as in [11], the system has been linearized by considering the speed as output, which is a procedure that allows the linearization of the whole electromechanical system. This assumption implies that the speed and flux are controlled without direct control of the stator current (equivalently of the torque), which is considered an internal variable. The idea is to design a controller permitting the flux and speed to be controlled with the best dynamic performance, without any coupling both in steady state and in dynamic conditions between the two loops and avoiding, at the same time, current, or torque controllers. A quite different approach is proposed in [24], where the stator currents are considered as the output of the system, and thus, are directly controlled. This leads to a different strategy because only the electrical part of the system can be linearized, and the speed must be managed by means of a further external loop (typically adopting a PI controller).

The proposed ADRC controller has been compared experimentally with the field-oriented control [specifically with the rotor oriented control (ROC)], because it can be considered the industrial standard for the high-performance control of

SynRM drives, and with the FLC for at least two reasons: 1) because it is a model-based control technique that can be viewed as a generalization of the field-oriented control [5], guaranteeing decoupled control of speed and flux loops in variable flux working conditions, whereas field-oriented control cannot, 2) because ADRC can be viewed as an upgraded version of the FLC, where the nonlinear transformations of the state and the input necessary for guaranteeing decoupled control of the flux and speed loops is not performed on the basis of an a priori known dynamic model of the SynRM, but on the basis of an ESO performing the online estimation of the compensation term. To make a more meaningful comparison, the authors have chosen a further high-performance control technique with which the proposed ADRC has been experimentally compared: the finite-state model predictive control (MPC). Such a control technique has been chosen for some reasons: 1) MPC is a model-based control technique and, from this point of view, it belongs to the same category of the proposed ADRC, 2) the finite set MPC generates as a control variable a reference value of stator voltage space vector (provided to a pulsewidth modulation (PWM)) and, from this point of view, it is comparable with the proposed ADRC, whereas the continuous state MPC seems to the authors hardly comparable with the proposed ADRC, 3) MPC is probably among the most studied high-performance control techniques of electric drives in these last years. In particular, the finite set MPC, proposed by the authors themselves in [25], has been adopted, where the speed control loop has been integrated into the framework of the MPC technique. This has been made with the specific scope of verifying the interaction between the flux and speed controls in the framework of a unique controller, as in the ADRC case.

This article represents the improvement and evolution of [26].

A. COMPARISON WITH SCIENTIFIC LITERATURE

The most recent proposal of control techniques of synchronous motor drives, in particular SynRM drives, are in the framework of MPC [27], [27], [28], [29], and specifically devoted to current control. Such references are not listed here since, even if very interesting and up to date, they are not coherent with the proposed approach which is based on the decoupled flux and speed control, without any internal current control. The most recent applications of MPC to speed control of synchronous motors have been proposed in [30] and [31]. Otherwise, former proposals have been published in [32] and [33]. In particular, Gao et al. [30] proposed a direct MPC where a sliding manifold term is added to the cost function to realize the speed/current tracking; in particular, the prediction of the speed is performed on the basis of a discretized mechanical model, where the load torque is online estimated by a Kalman filter. In [30], two cost functions have been defined, containing both steady-state and transient terms as well as some constraint-based terms. This approach is comparable to the proposed ADRC as for the controlled variables, while it is hardly comparable from the control variables point of view, since the direct approach implies the direct selection of the VSI switching pattern. Liu et al. [31] proposed a continuous control set predictive speed control (CCS-PSC) strategy for surface-mounted permanent magnet synchronous motor (SPMSM) drives, where a reduced-order incremental model of SPMSM is adopted for the prediction; in this approach, constraints on the variables are naturally accounted for. Also this approach is hardly comparable to the proposed ADRC for at least two reasons. First, the machine under test is an SPMSM, implying an almost negligible saliency and saturation effect. This justifies the adoption of a simplified reduced-order model: such an approach could not be adopted in the SynRM case, where accurate modeling, including magnetic saturation phenomena, is crucial for guaranteeing high dynamic performance. Second, Liu et al. [31] proposed an approach implying the direct selection of the VSI switching pattern, differently from the proposed ADRC providing as a control variable the stator voltage components supplied to a PWM. Ding et al. [34] proposed a second-order sliding mode (SOSM) controller based on disturbance observer (DOB) to optimize the disturbance rejection property of the PMSM system. Also this approach is hardly comparable to the proposed ADRC, since the proposed approach modifies only the structure of the speed controller, while the structure of the nested current controllers classic of field-oriented control is still present in the overall control scheme. Lin et al. [35] proposed a speed control system based on the two-degree-of-freedom (2DOF) structure. Also this approach is hardly comparable to the proposed ARDC, since it modifies only the structure of the speed controller, while the structure of the nested current controllers classic of field-oriented control is still present in the overall control scheme. To the best of the author's knowledge, the only application of ADRC to *SynRM* drives in [36] presents an active disturbance rejection current control scheme for SynRM drives. In particular, he designed two identical control loops that manage the current of an SynRM motor in order to make the current control robust to magnetic saturation and winding temperature. However, it does not investigate the speed and the flux control. This article proposes a complete scheme where the inputs are not current references but the flux ψ_s and the rotor speed, while the current control is embedded in the proposed scheme. This improves robustness beyond magnetic saturation, winding temperature, and mechanical parameters, such as friction and inertia moment. Finally, Li et al. [36] presented only simulation results, while the proposed strategy is validated experimentally. In the authors' opinion, the above considerations justify the innovative contribution of the proposed *ADRC*.

II. IMPACT OF SELF- AND CROSS-SATURATION ON THE *SYNRM* DYNAMICAL MODEL

This section is devoted to the description of the dynamic model of the SynRM, including magnetic saturation (both self and cross saturation). The magnetic model of the SynRM is here described only for clarity of reading in order to emphasize the complexity and computational requirement of a

model-based controller relying on such a model (e.g., *FLC* in [11]). It should be, however, stressed that the knowledge of such a model is not required at all in the proposed ADRC since the nonlinear correction terms are estimated online by ESOs, as fully described in the following.

The magnetic behavior of SynRMs has been addressed in the scientific literature mainly with current versus flux approaches. In particular, accurate models consider both self and cross-saturation. Among the few dynamic models based on the flux versus current approach, the model proposed in [37] has been developed starting from a suitably conceived coenergy variation function and considers both self and cross-saturation phenomena, fulfilling the reciprocity conditions, as required by the physics of the system.

Let us consider the state variables of the SynRM, that are the space vector of the stator flux, $\boldsymbol{\Psi}_s = [\psi_{sx},\ \psi_{sy}]$, and the space vector of the stator current, $\mathbf{i}_s = [i_{sx},\ i_{sy}]$, expressed in the rotor reference frame. The following first equation can be written:

$$\frac{d\boldsymbol{\Psi}_s}{dt} = \mathbf{u}_s - R_s\mathbf{i}_s - j\omega_r\boldsymbol{\Psi}_s. \tag{1}$$

As shown in [37], the stator fluxes can be obtained from the stator current using the following relations:

$$\psi_{sx} = L_{sxx}i_{sx}, \quad \psi_{sy} = L_{syy}i_{sy} \tag{2}$$

where the direct and quadrature components of the static inductances can be expressed as [37]

$$L_{sxx} = \frac{\Psi_{sx}}{i_{sx}} = \frac{\alpha_1 \tanh(\beta_1 i_{sx})}{i_{sx}} + \eta_1 + \\ - \frac{\gamma}{4}\frac{\operatorname{sign}(i_{sx})}{i_{sx}}\frac{\tanh\left(\frac{(i_{sy}-\mu_2\operatorname{sign}(i_{sy}))}{\sigma_2}\right)\cdot\operatorname{sign}(i_{sy})+1}{\sigma_1 i_{sx}\cosh^2\left(\frac{(i_{sx}-\mu_1\operatorname{sign}(i_{sx}))}{\sigma_1}\right)} \tag{3a}$$

$$L_{syy} = \frac{\Psi_{sy}}{i_{sy}} = \frac{\alpha_2 \tanh(\beta_2 i_{sy})}{i_{sy}} + \eta_2 + \\ - \frac{\gamma}{4}\frac{\operatorname{sign}(i_{sy})}{i_{sy}}\frac{\tanh\left(\frac{(i_{sx}-\mu_1\operatorname{sign}(i_{sx}))}{\sigma_1}\right)\cdot\operatorname{sign}(i_{sx})+1}{\sigma_2 i_{sy}\cosh^2\left(\frac{(i_{sy}-\mu_2\operatorname{sign}(i_{sy}))}{\sigma_2}\right)}. \tag{3b}$$

The above functions (3a) and (3b), which are linked to the magnetic description of the SynRM, require the knowledge of 11 parameters. Moreover, as highlighted in [37], the reciprocity conditions required by the cross-saturation are inherently met so that the inductances (3a) and (3b) are not energy sources or sinks.

By introducing (2) into (1) and considering (3a) and (3b), the following equation, expressed in state form, can be obtained, where the stator currents are chosen as state variables

$$\frac{d\mathbf{i}_s}{dt} = \mathbf{L}_s'^{-1}(\mathbf{u}_s - R_s\mathbf{i}_s - j\omega_r\mathbf{L}_s\mathbf{i}_s) \tag{4}$$

where $\mathbf{L}_s'^{-1}$ is defined as

$$\mathbf{L}_s'^{-1} = \frac{1}{L'_{sxx}L'_{syy} - L'_{sxy}L'_{syx}}\begin{bmatrix} L'_{sxx} & L'_{syx} \\ L'_{sxy} & L'_{syy}\end{bmatrix}. \tag{5}$$

The matrix coefficients on the left-hand side of (5) are the self and cross-dynamic inductances and are given as (6) shown at the bottom of the next page. The last equation of the state model is, as usual, represented by the mechanical equation

$$J\frac{d\omega_r}{dt} = -f_v\omega_r + t_m - t_l \tag{7}$$

where J is the moment of inertia, f_v the viscous friction, t_l the load torque, and t_m is the electromagnetic torque expressed as

$$t_m = \frac{3}{2}p\left(L_{sxx} - L_{syy}\right)i_{sx}i_{sy} = \frac{3}{2}p\left(\frac{1}{L_{sxx}} - \frac{1}{L_{syy}}\right)\psi_{sx}\psi_{sy}. \tag{8}$$

In particular, the electromagnetic torque (8) depends only on the static inductances directly, and on the dynamical inductances indirectly via the stator flux components.

III. ACTIVE DISTURBANCE REJECTION CONTROL LAW

Assume that the SynRM drive is operated under ROC or FOC or any FLC not involving the speed loop in the controller design. If the controlled variables are the direct axis current (or the stator flux or the active flux) and the rotor speed, assuming that the drive is operated under MTPA, the speed and the direct axis control loops are coupled by the torque expression (8). As for the coupling between the speed and flux loops, the following considerations should be made. In IM drives, such coupling exists between the speed and the rotor flux loops. In this case, the rotor flux loop bandwidth is governed by the rotor time constant, which is much higher than the stator transient time constant usually governing the dynamic of the current loops, even if it is still much lower than the speed bandwidth. This coupling, even if the rotor time constant is much lower than the mechanical time constant of the machine governed by its inertia, fully justifies the adoption of FLC or ADRC for decoupling speed and flux loops in transient flux working condition. In the SynRM case, the flux loop presents the same dynamics as the direct current loop which is still much slower than that of the mechanical system. The above consideration fully justifies the adoption of the FLC or ADRC in SynRM drives for improving the dynamic performance under variable flux conditions.

The only way to decouple the speed and direct axis current loops is to adopt a suitably defined nonlinear controller accounting for the mechanical dynamic equation of the motor. In [11], the FLC approach has been followed; in this article, an original ADRC approach is presented.

An extended model will be used if ADRC is adopted. This is achieved by introducing another state variable representing the total disturbance acting on the system. It permits the dynamical model to be written as a chain of integrators, that is in canonical form. The total disturbance is observed by an ESO technique, and then a control law is synthesized. As will

appear clear in the following, this comprises two components whose tasks are to adaptively compensate for the total disturbance and follow the reference, respectively.

A. EXTENDED MODELS

The proposed algorithm adopts two extended models: one for the flux on the quadrature axis (flux extended model) and one for the speed (speed extended model).

1) FLUX EXTENDED MODEL

This model can be derived by using equations (1)–(4) linearizing, as in [11], with $x_{\psi 1} = \psi_{sx}$

$$\dot{x}_{\psi 1} = f_{\psi} + u_{sx} \tag{9}$$

where f_{ψ}, the *total flux disturbance*, is defined as

$$f_{\psi} = -R_s i_{sx} + \omega_r \psi_{sy}. \tag{10}$$

By defining another state variable $x_{\psi 2} = f_{\psi}$, the flux extended model can be written as

$$\dot{x}_{\psi 1} = x_{\psi 2} + u_{sx}, \qquad \dot{x}_{\psi 2} = \dot{f}_{\psi}. \tag{11}$$

2) SPEED EXTENDED MODEL

This model is derived like the flux extended model, assuming that the speed is a measured output and $\dot{\imath}_l \approx 0$. In this case, from the model equations (1)–(4) and (7) and (8), and the linearization employed in [11], and defining $x_{\omega 1} = \omega_r$ and $x_{\omega 2} = \dot{\omega}_r = a$, the following equations can be derived:

$$\dot{x}_{\omega 1} = x_{\omega 2}, \qquad \dot{x}_{\omega 2} = f_{\omega} + b_{\omega} u_{sy} \tag{12}$$

where f_{ω} is called *total speed disturbance* defined as follows:

$$f_{\omega} = -f_v a + \frac{3p}{2J}\left(\begin{bmatrix} g_1 & g_2 \end{bmatrix} \mathbf{L}_s'^{-1} + \left(\frac{1}{L_{sxx}} - \frac{1}{L_{syy}} \right) \begin{bmatrix} \psi_{sx} & \psi_{sy} \end{bmatrix} \right) \begin{bmatrix} u_{sx} - R_s i_{sx} + \omega_r \psi_{sy} \\ -R_s i_{sy} - \omega_r \psi_{sx} \end{bmatrix} \tag{13}$$

where

$$g_1 := \left(\frac{\frac{\partial L_{sxx}}{\partial i_{sx}}}{L_{sxx}^2} - \frac{\frac{\partial L_{syy}}{\partial i_{sx}}}{L_{syy}^2} \right) = \frac{1}{i_{sx}} \left(\frac{L'_{sxx} - L_{sxx}}{L_{sxx}^2} \right) + \frac{1}{i_{sy}} \left(\frac{L'_{syx}}{L_{syy}^2} \right) \tag{14a}$$

$$g_2 := \left(\frac{\frac{\partial L_{sxx}}{\partial i_{sy}}}{L_{sxx}^2} - \frac{\frac{\partial L_{syy}}{\partial i_{sy}}}{L_{syy}^2} \right) = \frac{1}{i_{sy}} \left(\frac{L'_{syy} - L_{syy}}{L_{syy}^2} \right) + \frac{1}{i_{sx}} \left(\frac{L'_{sxy}}{L_{sxx}^2} \right) \tag{14b}$$

while b_{ω} is defined as

$$b_{\omega} = \frac{3p}{2J} \left(\frac{g_1 L'_{sxy} + g_2 L'_{syy}}{L'_{sxx} L'_{syy} - {L'_{sxy}}^2} + \left(\frac{1}{L_{syy}} - \frac{1}{L_{sxx}} \right) \psi_{sx} \right). \tag{15}$$

Also in this case, if an extra state variable $x_{\omega 3} = f_{\omega}$ is defined, the speed extended model becomes

$$\dot{x}_{\omega 1} = x_{\omega 2}, \qquad \dot{x}_{\omega 2} = x_{\omega 3} + b_{\omega} u_{sy}, \qquad \dot{x}_{\omega 3} = \dot{f}_{\omega}. \tag{16}$$

Models (11) and (16) show that the flux and speed extended models have the same structure but different dimensions. Moreover, choosing the control variables as follows:

$$u_{sx} = -\hat{x}_{\psi 2} + \nu'_x, \qquad u_{sy} = \frac{1}{b_{\omega}} \left(-\hat{x}_{\omega 3} + \nu'_y \right) \tag{17}$$

where $\hat{x}_{\psi 2}$ and $\hat{x}_{v3}$ are the estimates of $x_{\psi 2}$ and x_{v3}, respectively, and designing ν'_x and ν'_y so that the models (11) and (16) satisfy the design requirements, the total disturbances can be assumed as perfectly compensated. Two ESOs are then used to estimate the total disturbances. Specifically, the estimation of the total disturbance is obtained by estimating the second state variable in the extended flux model and the third state variable in the speed model.

Remark 1: The differences between this ADRC and the FLC in [11] (with which it will be compared in the following) are, therefore:

1) in the FLC in [11], the control inputs are formally the same as (17), but the total disturbances $f_{\psi} = x_{\psi 2}$ and $f_{\omega} = x_{\omega 3}$ are obtained analytically exploiting (10) and (13). This computation, however, is affected by the modeling errors and the related parameter uncertainty, compounded by the involved expressions (10) and (13);

$$L'_{sxx} = \frac{d\Psi_{sx}}{di_{sx}} = \frac{\alpha_1 \beta_1}{\cosh^2(\beta_1 i_{sx})} + \eta_1 + \frac{\gamma}{2\sigma_1^2} \frac{\operatorname{sign}(i_{sx}) \tanh\left(\frac{(i_{sx} - \mu_1 \operatorname{sign}(i_{sx}))}{\sigma_1} \right) \left[\tanh\left(\frac{(i_{sy} - \mu_2 \operatorname{sign}(i_{sy}))}{\sigma_2} \right) \cdot \operatorname{sign}(i_{sy}) + 1 \right]}{\cosh^2\left(\frac{(i_{sx} - \mu_1 \operatorname{sign}(i_{sx}))}{\sigma_1} \right)} \tag{6a}$$

$$L'_{syy} = \frac{d\Psi_{sy}}{di_{sy}} = \frac{\alpha_2 \beta_2}{\cosh^2(\beta_2 i_{sy})} + \eta_2 + \frac{\gamma}{2\sigma_2^2} \frac{\operatorname{sign}(i_{sy}) \tanh\left(\frac{(i_{sy} - \mu_2 \operatorname{sign}(i_{sy}))}{\sigma_2} \right) \left[\tanh\left(\frac{(i_{sx} - \mu_1 \operatorname{sign}(i_{sx}))}{\sigma_1} \right) \cdot \operatorname{sign}(i_{sx}) + 1 \right]}{\cosh^2\left(\frac{(i_{sy} - \mu_2 \operatorname{sign}(i_{sy}))}{\sigma_2} \right)} \tag{6b}$$

$$L'_{sxy} = \frac{d\Psi_{sx}}{di_{sy}} = L'_{syx} = \frac{d\Psi_{sy}}{di_{sx}} = -\frac{\gamma \operatorname{sign}(i_{sx}) \operatorname{sign}(i_{sy})}{4\sigma_1 \sigma_2 \cosh^2\left(\frac{(i_{sx} - \mu_1 \operatorname{sign}(i_{sx}))}{\sigma_1} \right) \cosh^2\left(\frac{(i_{sy} - \mu_2 \operatorname{sign}(i_{sy}))}{\sigma_2} \right)}. \tag{6c}$$

2) no a priori knowledge is necessary with ADRC to compute these terms online, avoiding any issue due to parameter uncertainty or unmodeled dynamics;
3) the use of ADRC introduces, besides the dynamics of the flux and speed loops, the dynamics of ESOs.

In synthesis, it can be stated that in constant flux operation ($i_{sx} = \text{const}$), the expected dynamic performance of the stator currents, electromagnetic torque, and speed responses achieved with the proposed ADRC cannot theoretically be much different from those achievable with the classic FOC. On the contrary, in variable flux operation (e.g., under MTPA), the expected dynamic performance will certainly be better than those of FOC, but they cannot be theoretically better than those achieved with the FLC. Performance achieved with the ADRC can at least be equal to those of the FLC, given that the model underlying it is absolutely accurate and its parameters perfectly tuned. It should be noted, however, that under detuned working conditions, the performance of FLC deteriorates significantly, becoming much lower than ADRC and often also than FOC. Therefore, the ADRC permits dynamic performance almost equal to those achievable with FLC but characterized by much higher robustness versus parameters' variations. This is because the correction terms of the controller are not a priori given based on the model, while they are estimated online by the ESO.

B. ESO FOR A THIRD-ORDER EXTENDED MODEL

This section will describe ESOs for both speed and flux extended models.

The ESO chosen for the state estimation of model (16) follows the one presented in [38], whose set of equations is given by

$$\dot{\hat{x}}_{\omega 1} = \hat{x}_{\omega 2} - \epsilon \beta_1 \left(\frac{\hat{x}_{\omega 1} - x_{\omega 1}}{\epsilon^2} \right) \tag{18a}$$

$$\dot{\hat{x}}_{\omega 2} = \hat{x}_{\omega 3} - \beta_2 \left(\frac{\hat{x}_{\omega 1} - x_{\omega 1}}{\epsilon^2} \right) + b_\omega u_{sy} \tag{18b}$$

$$\dot{\hat{x}}_{\omega 3} = -\epsilon^{-1} \beta_3 \left(\frac{\hat{x}_{\omega 1} - x_{\omega 1}}{\epsilon^2} \right) \tag{18c}$$

where ϵ is a suitable positive parameter, and $\beta_i(\cdot),\ i = 1, 2, 3$, are suitably chosen function.

If the estimation errors are given by $e_i = \hat{x}_{\omega i} - x_{\omega i},\ i = 1, 2, 3$, and defining

$$\rho_i = \frac{e_i}{\epsilon^{3-i}},\ i = 1, 2, 3 \tag{19}$$

the dynamics of the variables ρ_i are described by

$$\epsilon \ddot{\boldsymbol{\rho}} = \boldsymbol{A}\boldsymbol{\rho} + \epsilon \boldsymbol{b} \dot{f}_\omega \tag{20}$$

where $\boldsymbol{\rho} = \begin{bmatrix} \rho_1 & \rho_2 & \rho_3 \end{bmatrix}^T$, $\boldsymbol{A} = \begin{bmatrix} -\beta_1 & 1 & 0 \\ -\beta_2 & 0 & 1 \\ -\beta_3 & 0 & 0 \end{bmatrix}$, and $\boldsymbol{b} = \begin{bmatrix} 0 & 0 & -1 \end{bmatrix}^T$.

If the coefficients β_i are chosen such that matrix $\boldsymbol{A}$ is Hurwitz, and if the derivative of the total speed disturbance is bounded, then the estimation errors (19) converge to zero exponentially, as shown in [38].

Second-order dynamics can be considered for the flux extended model instead of a third-order one. For this reason, the ESO chosen for the state estimation of model (12) is given by

$$\dot{\hat{x}}_{\psi 1} = \hat{x}_{\psi 2} - \beta_1 \left(\frac{\hat{x}_{\psi 1} - x_{\psi 1}}{\epsilon} \right) + b_\psi u_{sx} \tag{21a}$$

$$\dot{\hat{x}}_{\psi 2} = -\epsilon^{-1} \beta_2 \left(\frac{\hat{x}_{\psi 1} - x_{\psi 1}}{\epsilon} \right) \tag{21b}$$

where ϵ is a suitable positive parameter, and the functions $\beta_i(\cdot),\ i = 1, 2$, are chosen like those used for the speed ESO.

C. DESIGN OF FLUX AND SPEED CONTROLLERS

Considering (16), if the control input is selected as in (17), and considering that $\hat{x}_{\omega 3} \approx x_{\omega 3}$, then the following model is obtained:

$$\dot{x}_{\omega 1} = x_{\omega 2}, \qquad \dot{x}_{\omega 2} = \nu_y'. \tag{22}$$

This corresponds to a double integrator, while in the case of the flux model, a single integrator is obtained: $\dot{x}_{\psi 1} = \nu_x'$. A state feedback controller based on the assignment of the eigenvalues can then be designed for model (22). However, steady-state null tracking errors are to be obtained. For good tracking of the reference, the state of model (22) is increased by using a third variable z, whose dynamics is

$$\dot{z}_\omega = x_{1\omega \text{ref}} - x_{\omega 1} \tag{23}$$

where $x_{1\omega \text{ref}}$ is the reference value of speed. Model (22)–(27) is reachable and the control law

$$\nu_y' = -\boldsymbol{k}_\omega^T \boldsymbol{x} \tag{24}$$

with $\boldsymbol{k}_\omega = \begin{bmatrix} k_{\omega 1} & k_{\omega 2} & k_{\omega 3} \end{bmatrix}^T$ and $\boldsymbol{x} = \begin{bmatrix} x_{\omega 1} & x_{\omega 2} & z_\omega \end{bmatrix}^T$, allows the eigenvalues of the dynamic matrix of the model to be assigned. The characteristic polynomial is given by

$$\Delta_\omega(\lambda) = \lambda^3 + k_{\omega 1}\lambda^2 + k_{\omega 2}\lambda + k_{\omega 3} \tag{25}$$

where the parameters $k_{\omega 1}, k_{\omega 2}$, and $k_{\omega 3}$ are determined assuming that the desired zeros of (25) are with negative real part. In order to implement the above control law, the state estimated by the ESO is necessary. In particular, the implementation of the control law requires the knowledge of $x_{\omega 1}$ and $x_{\omega 2}$, while the knowledge of $x_{\omega 3}$ allows the total disturbance f_ω to be compensated.

As for the flux model (16), the controller can be designed similarly to the speed controller. Specifically, by considering the control input given in (17) and $\hat{x}_{\psi 2} \approx x_{\psi 2}$, the following dynamics results:

$$\dot{x}_{\psi 1} = \nu_x'. \tag{26}$$

This is an integrator that is reachable; consequently, a state feedback controller can be designed based on the assignment of the eigenvalues. Also in this case, to obtain an unbiased tracking error, the state dimension is increased by adding a

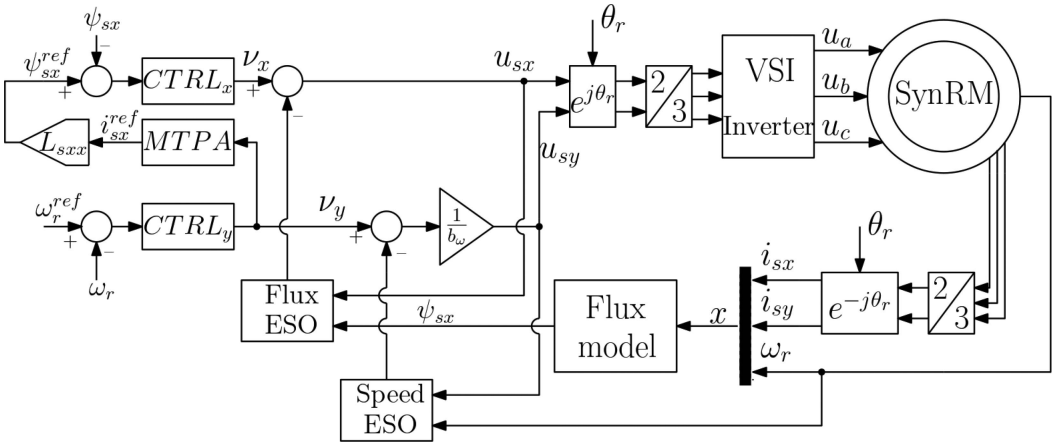

FIGURE 1. Block diagram of the proposed control algorithm.

second variable z_ψ, so that

$$\dot{z}_\psi = x_{1\psi\,\mathrm{ref}} - x_{\psi 1} \tag{27}$$

where $x_{1\psi\,\mathrm{ref}}$ is the reference flux. Thus, the control law

$$\nu_x' = -\boldsymbol{k}_\psi^T \boldsymbol{x} \tag{28}$$

with $\boldsymbol{k}_\psi = \begin{bmatrix} k_{\psi 1} & k_{\psi 2} \end{bmatrix}^T$ and $\boldsymbol{x} = \begin{bmatrix} x_{\psi 1} & z_\psi \end{bmatrix}^T$, allows the zeros of the characteristic polynomial of the direct axis flux

$$\Delta_\psi(\lambda) = \lambda^2 + k_{\psi 1}\lambda + k_{\psi 2} \tag{29}$$

to be assigned.

The block diagram of the proposed control algorithm is shown in Fig. 1.

Remark 2: This control strategy requires the existence of the inverse of b_ω. This can be ensured if ψ_{sx} is different from zero: however, this constraint corresponds to a physical characteristic of the *SynRM*, given that the motor works only if ψ_{sx} is higher than zero in any possible working conditions, so this condition is always satisfied.

Remark 3: Note that the auxiliary input ν_x appears in the definition of the total disturbance f_ω. This creates an interdependence between the linearized speed and flux models, making the proposed ADRC not standard and different from other applications proposed in the literature. This problem arises from the dependence on the self and cross-saturation inductances of the model from the stator current.

D. CLOSED-LOOP DYNAMICS

If the ESO dynamic is sufficiently fast, the characteristic polynomials (25) and (29) approximate very well the closed-loop dynamics of the speed and of the direct axis flux, respectively. This means that the controller coefficients can be suitably chosen to assign bandwidth and phase margin specifications.

In particular, for the speed dynamics, the parameters $k_{\omega 1}$, $k_{\omega 2}$, and $k_{\omega 3}$ can be determined assuming that the desired zeros of (25) are $\lambda_{\omega 1} = -\zeta\omega_n + j\omega_n\sqrt{1-\zeta^2}$, $\lambda_{\omega 2} = -\zeta\omega_n - j\omega_n\sqrt{1-\zeta^2}$, and $\lambda_{\omega 3} = \sigma$, where ω_n and ζ are the natural frequency and the damping factor, respectively, while σ is a negative constant. Therefore, if $|\sigma| >> \omega_n$, parameters ζ is directly linked with the phase margin by the relation

$$m_\phi = \frac{\pi}{2} - \tan^{-1}\left(\frac{\sqrt{-2\zeta^2 + \sqrt{4\zeta^4+1}}}{2\zeta}\right) \tag{30}$$

and, once ζ is fixed, the ω_n is directly linked with the bandwidth by the relation

$$\omega_n = \frac{B_{3db}}{\sqrt{1 - 2\zeta^2 + \sqrt{2 - 4\zeta^2 + 4\zeta^4}}}. \tag{31}$$

For the direct axis flux dynamics, parameters $k_{\psi 1}$ and $k_{\psi 2}$ of (29) are determined by assuming that the desired eigenvalues are $\lambda_{\psi 1} = -\zeta\omega_n + j\omega_n\sqrt{1-\zeta^2}$ and $\lambda_{\psi 2} = -\zeta\omega_n - j\omega_n\sqrt{1-\zeta^2}$, where ω_n and ζ are the natural frequency and the damping factor, respectively. As for the speed dynamics, ζ and ω_n can be chosen to assign bandwidth and phase margin with the help of (30) and (31). Note that the approximation $|\sigma| >> \omega_n$ is no longer needed for the direct axis flux dynamics since the system is actually second order.

This choice of controller parameters allows meaningful comparison with other control strategies, as shown in Section III-E, where all control strategies have been tuned with the same phase margin and bandwidth.

It is very important to note that, in order to make the ESO dynamics sufficiently fast with respect to the controller, and consequently to make the above approximation effective, it is necessary to choose $\epsilon << 1$ and coefficients β_i of matrix $\boldsymbol{A}$, in (20), such that the zeros of polynomials

$$\Delta_{\mathrm{ESO}-\omega}(\lambda) = \lambda^3 + \beta_1\lambda^2 + \beta_2\lambda + \beta_3 \tag{32a}$$

$$\Delta_{\mathrm{ESO}-\psi}(\lambda) = \lambda^2 + \beta_1\lambda + \beta_2 \tag{32b}$$

are placed on the left-hand side of the complex plane, with respect to the zeros of polynomials (25) for the speed loop and (29) for the direct axis flux loop. Note that ϵ cannot be chosen very small to avoid the peaking problem [39, Ch. 14.5.1].

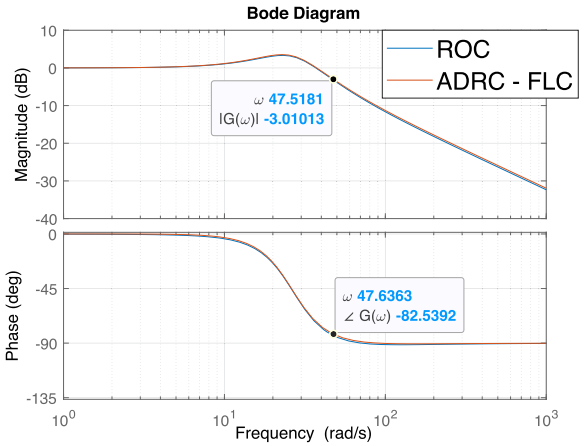

FIGURE 2. Bode Diagram: closed-loop transfer functions of the direct axis flux dynamics.

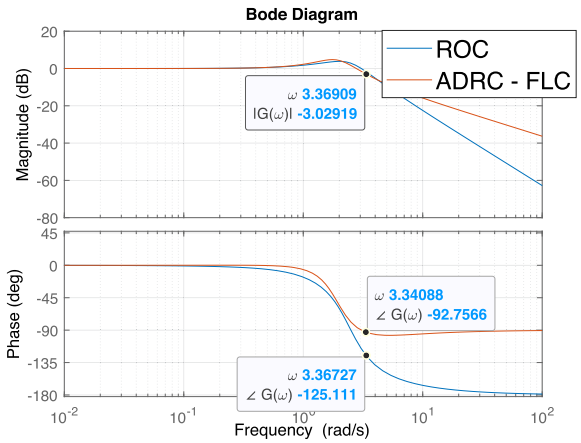

FIGURE 3. Bode Diagram: closed-loop transfer functions of the speed dynamics.

E. CONTROLLER DESIGN

To verify the improvements in the dynamic performance achievable with the adoption of the proposed control technique, it will be first compared with the industrial standard in high-performance control of SynRM drives: the field oriented control. Among the different FOC algorithms, the ROC has been adopted here for comparison purposes. Moreover, the proposed ADRC has been further compared with the FLC presented in [11]. In detail, the controller parameters ω_n, ξ, and σ (for both speed and flux loop), given in Section III-D (adopted both in the ADRC and the FLC), and the parameters of the PI in the ROC should be chosen so that the two closed-loop systems present the same dynamics. In this case, the same crossing pulsation $\bar{\omega}_t$ and the same phase margin $\bar{m}_\phi$ are imposed.

With this aim, for both ROC and ADRC, the Bode diagrams of the transfer functions of the closed-loop systems, plotted in Figs. 2 and 3, are obtained (the corresponding Bode diagrams of the FLC are not shown since they are superimposable to those of the ADRC). From these figures, it can be easily observed that the three systems, respectively, the SynRM controlled with ADRC, the FLC, and the ROC, have the same bandwidths equal, respectively, to 47.5 rad/s for the flux loop and 3.4 rad/s for the speed loop. Moreover, in correspondence with the cutoff frequency, the systems have the same phase, equal, respectively, to $-82.5\,^\circ$ for the flux loop; for the speed loop, a phase equal to $-92.7\,^\circ$ has been obtained in the ADRC and FLC cases, and $-125\,^\circ$ in the ROC case.

TABLE 1 Performance Indicators Related to Test in Fig. 6

	ADRC	FLC TUNED	FLC DETUNED
IAE	25.3	25.7	49.8
ITAE	4.96	5.22	13.83

However, to obtain the transfer functions in the ROC case, the assumptions of constant parameters and constant direct axis flux amplitude should be made. In particular, the parameters obtained at rated currents are considered for the transfer function of the flux and the transfer function of the speed. This represents a limitation for the ROC as compared with the ADRC and FLC, where the specifics are satisfied in all working conditions. In the ROC case, these specifics could change if the flux level is different from the rated one (condition always happening under MTPA). They are therefore rigorously respected in one only working condition.

In synthesis, analytical relationships between the controller gains and, from one side, the phase margin and, from the other side, the bandwidth of the system have been given. With the proposed approach, there is a direct analytical relationship between the system desired performance and the controller gains [see (29)–(31)]. An analytical methodology has also been proposed to ensure that the ESOs present a sufficiently fast dynamic. This methodology is described by (32). The selected values of 47.5 rad/s for the flux loop and 3.4 rad/s for the speed loop are chosen coherently with the values of the dynamic inductances of the motor (for the flux loop) and its inertia (for the speed loop). The stability of the system is intrinsically guaranteed by the control design procedure described in Section III-C, III-D, and III-E. Once the values of bandwidth for the flux and speed loops are selected, the phase margin of the system and the natural frequency are defined univocally by (30) and (31). This corresponds to selecting the zeros of the characteristic polynomials of the flux and speed loops; see (25) and (29). With regards to the stability proof of the ESO, it has been extensively treated in other literature works (see, for example, [12] and [13]) and, for this reason, was not repeated in this article.

IV. SIMULATION RESULTS

The performance of the proposed ADRC for SynRM drives has been initially tested in numerical simulation. As for the SynRM under test, the motor whose rated data are shown in Table 2 has been simulated in Matlab-Simulink environment. In the following, all the simulation and experimental tests have been performed by integrating into all the control

TABLE 2 Rated Data of the SynRM

SYMBOLS	VALUES
Rated power (kW)	2.2
Rated voltage (V)	380
Rated frequency (Hz)	50
Pole-pairs	2
Rated speed (rpm)	1500
Rated current (A)	5.5
Rated torque (Nm)	14
Inertia momentum (kg·m^2)	0.00351

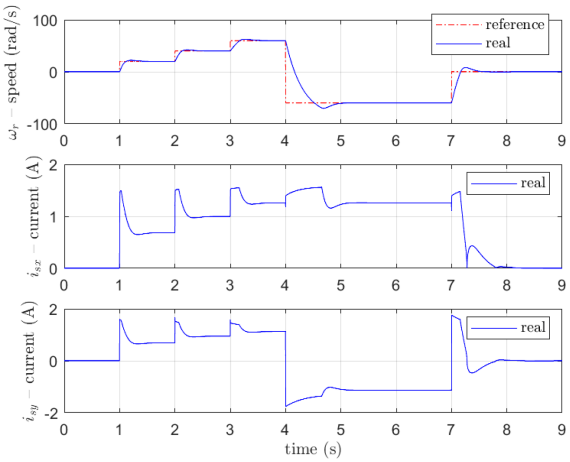

FIGURE 4. Reference and measured speed and i_{sx}, i_{sy} with the ADRC during the 0 → 20 → 40 → 60 → −60 → 0 rad/s at no load (simulation).

systems the MTPA technique proposed in [40]. A first numerical test has been made to verify the dynamic performance of the ADRC. In particular, a set of speed steps, including a speed reversal, of the type 0 → 20 → 40 → 60 → −60 → 0 rad/s at no load has been given in the SynRM drive. The same test has also been performed experimentally (see Figs. 8 and 9). Fig. 4 shows the reference and the measured speed of the SynRM drive as well as the corresponding i_{sx}, i_{sy} stator current waveforms under this test. The speed waveform shows the very high dynamic performance of the speed loop under very fast speed changes, with low rise times and zero steady-state tracking error. The i_{sy} waveform shows a spike-like shape, with spikes of positive/negative signs occurring at each variation of the reference speed, as expected, to accelerate the motor in both directions. The i_{sx} waveform shows a spike-like shape, with spikes of positive sign occurring contemporary to those of i_{sy}, as expected due to the adoption of the MTPA. It can be observed that the ADRC permits the i_{sx}, i_{sy} current components to be controlled in a decoupled way (exactly as ROC) and with very high dynamic performance.

A second numerical test is a load rejection test. In particular, the drive has been operated at the constant speed of 100 rad/s (almost 2/3 of the rated speed), and a load step torque of 10 Nm has been applied at 1 s and released at 6 s. The same test has also been performed experimentally (see Figs. 10 and 11). Fig. 5 shows the reference and the measured

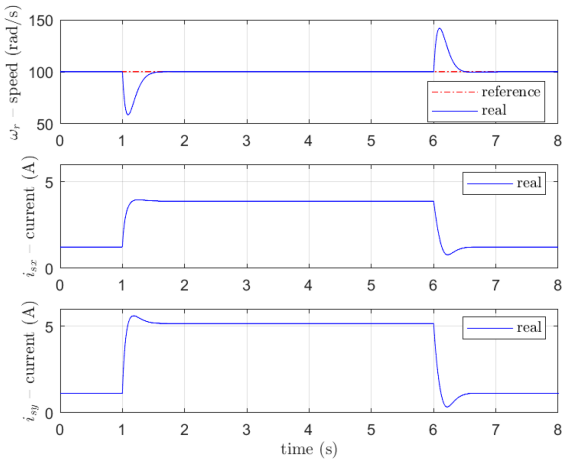

FIGURE 5. Reference and measured speed and i_{sx}, i_{sy} with the ADRC at high speed and high load torque (simulation).

speed of the SynRM drive as well as the corresponding i_{sx}, i_{sy} stator current waveforms under this test. The speed waveforms show a good load rejection capability of the controller even under variable flux working conditions; the speed controller can quickly cope with the application of the load torque, governing the measured speed to the reference in about 0.5 s, with steady-state null error. As for the waveforms of the direct and quadrature components of the stator current, i_{sy} presents a waveform almost proportional to the electromagnetic torque, as expected, with step changes occurring at each load step application. At the same time, i_{sx} is a time-varying quantity presenting almost the same shape of i_{sy}, given that the SynRM drive has been operated under MTPA.

A third numerical test has been made to verify the antidisturbing capability offered by the ADRC in dynamic working conditions. In this test, the SynRM drive runs at the constant speed of 60 rad/s at no load. It is supposed that, at $t = 1$ s, both the dynamic inductances of the SynRM are incremented instantaneously by 50%. The simulation test has been performed in three cases: 1) adoption of the ADRC, 2) adoption of the FLC with fixed parameters, and 3) adoption of the FLC in which the parameters adapted instantaneously to those of the SynRM. The obtained results, shown in Fig. 6, clearly highlight that the performance of the ADRC maintains almost the same, since the ESO can estimate the correction term correctly, even if the parameters of the SynRM vary suddenly. It is confirmed by the fact that the performance achieved with the ADRC is almost equal, or slightly better than those obtained with the FLC in which the parameters adapt instantaneously to those of the SynRM. On the contrary, this is not the case of the FLC with fixed parameters whose dynamic performance worsens consistently after the variation of the dynamic inductances. Table 1 shows the integral absolute error (IAE) and integral time absolute error (ITAE) indexes of the speed control loop for all the controllers . It can be easily observed that the IAE and ITAE indexes show an improved performance of the speed controller achievable with

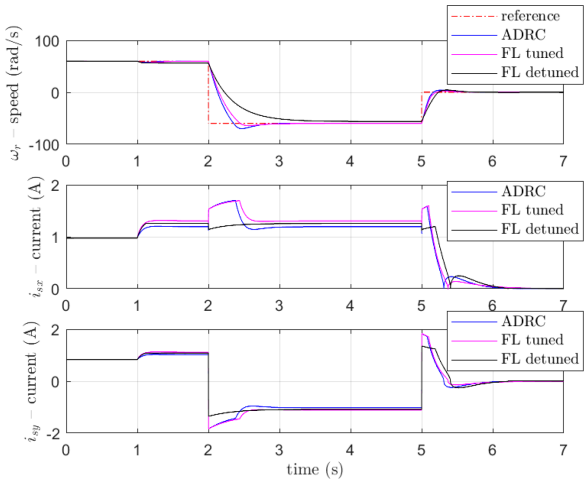

FIGURE 6. Reference and measured speed and i_{sx}, i_{sy} with the ADRC during the 60 → −60 → 0 rad/s at no load with varying SynRM parameters (simulation).

TABLE 3 Parameters of the *SynRM* Saturation Model

SYMBOL	VALUE	SYMBOL	VALUE
γ	0.1072	β_1	0.3044
μ_1	3.210	η_1	$1.0923 \cdot 10^{-2}$
μ_2	1.4380	α_2	0.1224
σ_1	0.6987	β_2	1.1125
σ_2	0.8023	η_2	$2.7329 \cdot 10^{-2}$
α_1	1.1627	R_0	8142

the proposed technique, in comparison with the FLC, both in the tuned and detuned versions.

V. EXPERIMENTAL TEST SETUP

The proposed ADRC has been tested experimentally on an experimental rig developed on purpose. The SynRM motor is the ABB 3GAL092543-BSB whose rated data are in Table 2. Table 3 shows the parameters of the complete saturation model, identified with the technique proposed in [37]. A PMSM is coupled with the SynRM, which works as an active load. The entire control algorithm has been implemented on a Dspace DS1103 board. The entire control system runs at a sampling frequency of 10 kHz. As for the PWM, a space-vector PWM with a switching frequency of 5 kHz has been adopted. Note that the 10-kHz running frequency of the control system is sufficient to ensure high performance of the SynRM drive, but the control algorithm could be executed much faster since it does not require a high computational effort. Typically, with the proposed hardware, it can run at 100–200 kHz, but it makes no sense to operate the drive at this high frequency. The voltage source inverters is based on Semikron IGBTs model SMK 50 GB 123 characterized by a threshold voltage of 1.2 V and a differential resistance of 0.02 Ω. Fig. 7 shows the photo of the SynRM drive test set-up.

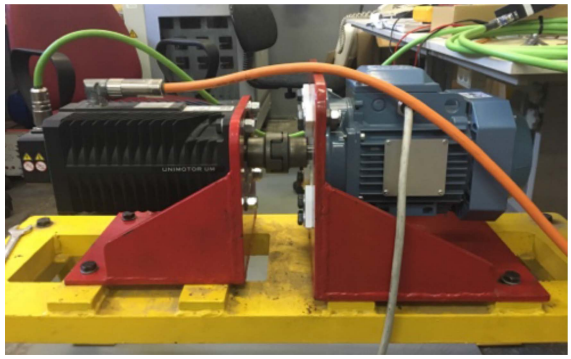

FIGURE 7. Photograph of the *SynRM* experimental set-up.

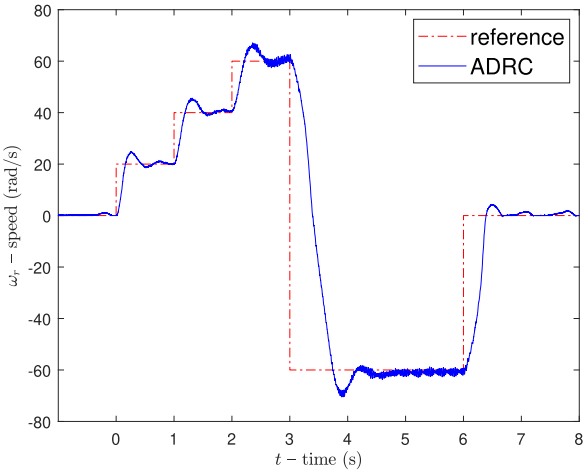

FIGURE 8. Reference and measured speed with the ADRC during the 0 → 20 → 40 → 60 → −60 → 0 rad/s at no load (experiment).

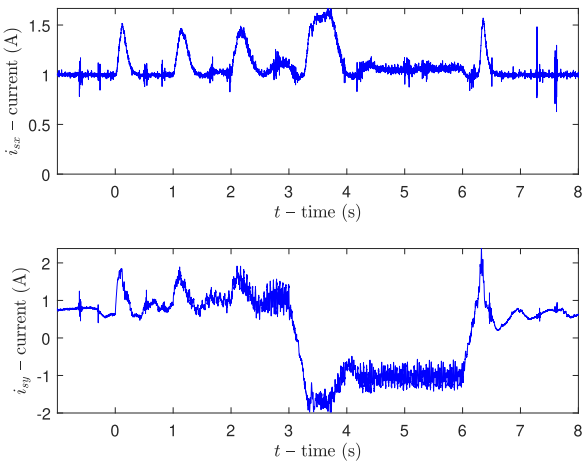

FIGURE 9. i_{sx} and i_{sy} with the ADRC during the 0 → 20 → 40 → 60 → −60 → 0 rad/s at no load (experiment).

VI. EXPERIMENTAL RESULTS

The first experimental test corresponds to the first simulation. Fig. 8 shows the reference and the measured speed of the SynRM drive while Fig. 9 shows the corresponding i_{sx}, i_{sy} stator current waveforms under this test.

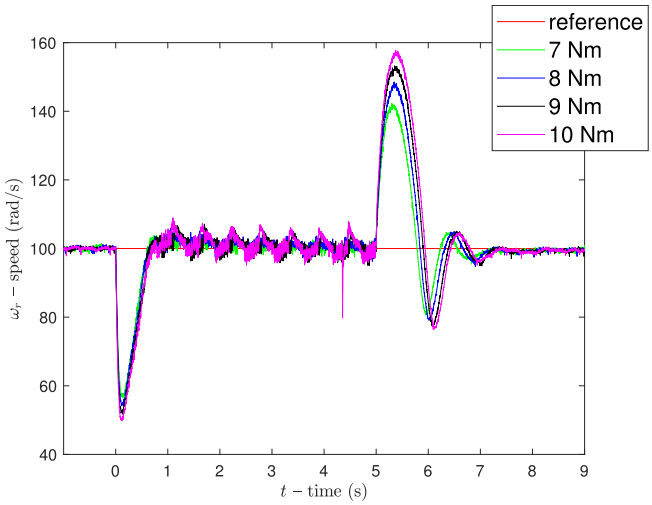

FIGURE 10. Reference and measured speed with the *ADRC* at high speed and high load torque (experiment).

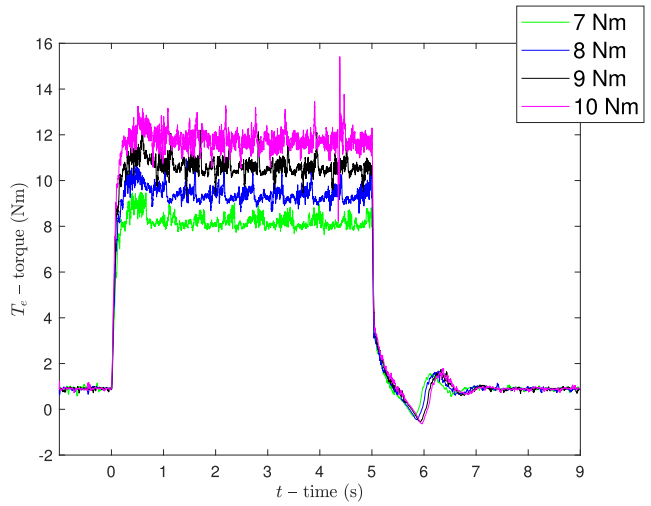

FIGURE 11. Load torque with the *ADRC* at high speed and high load torque (experiment).

The second experimental test corresponds to the second simulation. The experimental tests were repeated four times for increasing load torque values, respectively, 7, 8, 9, and 10 Nm (up to almost 2/3 of the rated torque). As for applying the load torque, the torque controlled PMSM drive described in Section IV has been exploited. Fig. 10 shows the reference and measured speed, Fig. 11 the electromagnetic torques, and finally Fig. 12 the direct and quadrature components of the stator current i_{sx}, i_{sy} during these tests. The experimental results confirm what was stated regarding the simulation results, showing excellent load rejection capability achievable with the proposed ADRC. The speed waveforms show a good load rejection capability of the controller even under variable flux working conditions; the speed controller can quickly cope with the application of the load torque, constantly governing the measured speed to the reference one in a time interval comprised between 0.5 and 1 s, with steady-state null error.

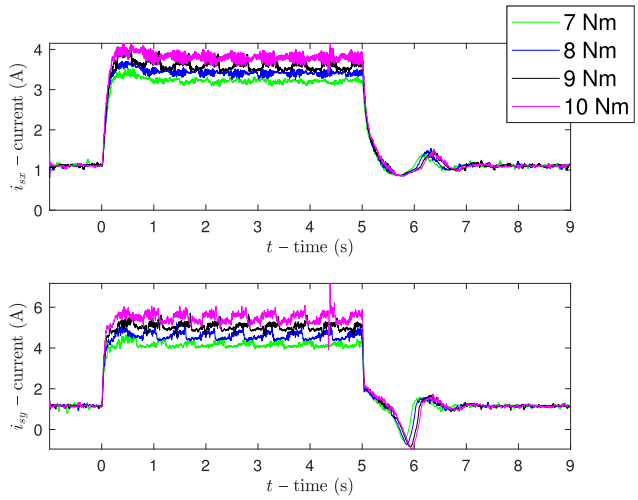

FIGURE 12. i_{sx} and i_{sy} with the ADRC at high speed and high load torque (experiment).

Moreover, it can be noticed that the speed overshoots and the recovering times are almost independent of the load torque values. The electromagnetic torque waveforms show a very fast torque response of the drive to the load application. The ADRC can control the generated torque from 0 to 2/3 of the rated load in about 0.18 s, independently from the value of the load and with almost no overshoot. As for the waveforms of the direct and quadrature components of the stator current, i_{sy} presents a waveform almost proportional to the electromagnetic torque, as expected, with step changes occurring at each load step application. At the same time, i_{sx} is a time-varying quantity presenting almost the same shape of i_{sy}, given that the SynRM drive has been operated under MTPA.

A. *COMPARISON BETWEEN* ADRC, FLC, ROC *AND* MPC

The ADRC is supposed to offer, at the same time, very high dynamic performance and robustness versus model/parameter uncertainty of the SynRM drive in variable flux working conditions. To show it, the proposed ADRC has been compared experimentally with both the classic ROC [40], with the FLC accounting for the magnetic saturation (both self and cross) presented in [11] and finally with the finite state MPC presented in [25], where, to make a more reasonable comparison, the speed control has been integrated in the MPC structure. In particular, to highlight the increase of robustness versus model/parameter uncertainty offered by ADRC compared with FLC, the FLC in [11] has been tested in both tuned and detuned working conditions, as better explained in the following.

The third experimental test corresponds to the third simulation. Fig. 13 shows the reference and the measured speed of the SynRM drive while Fig. 14 shows the corresponding i_{sx}, i_{sy} stator current waveforms under this test. The speed waveforms show that the best dynamic performance has been obtained by the correctly tuned FLC, followed by ADRC, ROC, and MPC. This is to be expected since, when the FLC

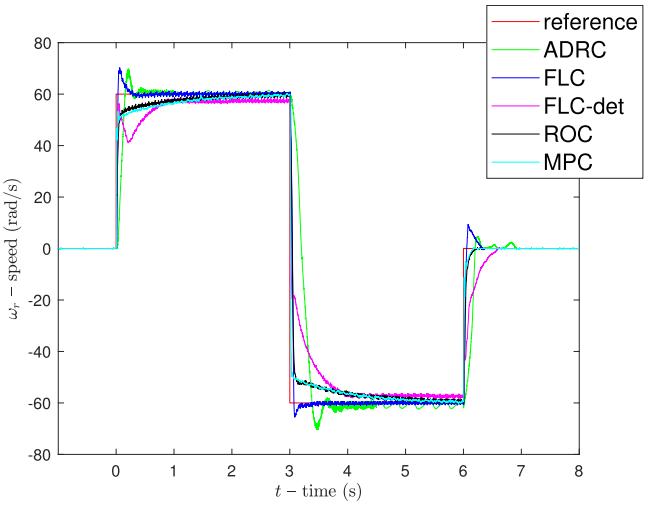

FIGURE 13. Reference and measured speed during the $0 \rightarrow 60 \rightarrow -60 \rightarrow 0$ rad/s at no load (experiment).

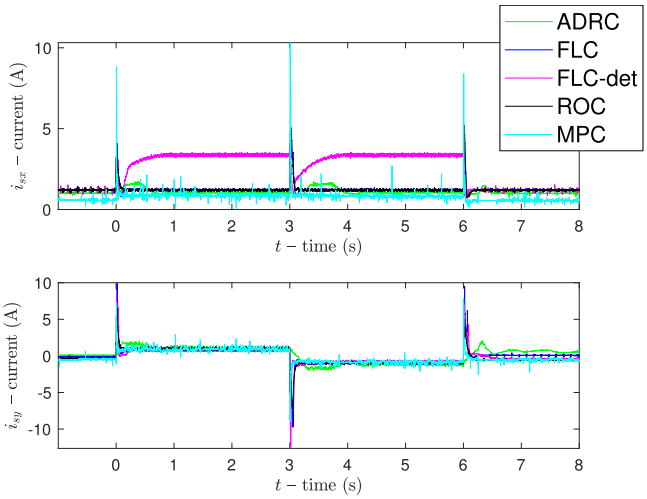

FIGURE 14. i_{sx}, i_{sy} during the $0 \rightarrow 60 \rightarrow -60 \rightarrow 0$ rad/s at no load (experiment).

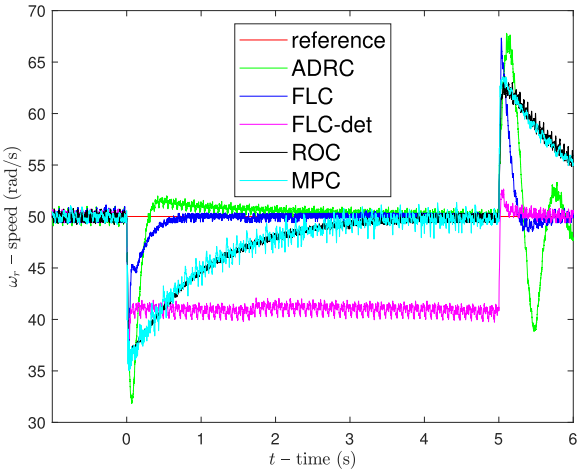

FIGURE 15. Reference and measured speed at constant speed of 50 rad/s with 5 Nm load step torque (experiment).

is correctly tuned, the nonlinear correction terms involving the input and state are accurate and do not introduce any dynamics. On the contrary, the same nonlinear correction terms involving the input and state are not a priori known in the ADRC, where they are online estimated with defined dynamics, which unavoidably slightly reduces the dynamic performance of the controller. The ROC presents, among the three controllers, the worse dynamic performance since the speed and flux loops are inherently coupled in variable flux working conditions (MTPA). MPC shows, as for the speed control, almost the same dynamic performance offered by ROC, witnessing that the coupling between the speed and flux loops still maintains in variable flux operation. The same speed waveform shows the trace of the FLC under detuned working conditions. Specifically, the FLC controller has been purposely detuned by considering a wrong value of the nonlinear state feedback of 30%. It can be seen that if FLC is not properly tuned, it presents dynamic performance worse than ROC and far worse than ADRC, which on the contrary, offers a good robustness thanks to the online estimation of the nonlinear correction terms. Moreover, the detuned FLC presents a nonnull speed steady-state tracking error, differently from the tuned FLC as well as ADRC and ROC. Consequently, the i_{sx}, i_{sy} waveforms in Fig. 14 present the expected spike-like shapes. The only waveform that is not consistent with the others is that of the detuned FLC, which presents completely different steady-state values of i_{sx}, i_{sy} at 60 rad/s; in particular, i_{sx} higher than 3 A is more than double than the corresponding value obtained with the other controllers. The above test confirms what is well known from the theoretical point of view. The ADRC cannot outperform FLC if it is perfectly tuned (accurate model and well-known parameters). In these working conditions, ADRC can perform at least like FLC, not better. ADRC outperforms FLC in conditions of varying parameters, in correspondence to which FLC becomes detuned and its performance drastically decrease.

As a second experimental comparative test, all the controllers have been tested at the constant speed of 50 rad/s with a load step torque of 5 Nm which is initially applied and then released. Fig. 15 shows the reference and the measured speed of the SynRM drive while Fig. 16 shows the corresponding i_{sx}, i_{sy} stator current waveforms under this test. The speed waveforms show that the best load rejection capability is obtained by the correctly tuned FLC, followed by ADRC, ROC, and MPC, as expected because of the above explained reasons. On the contrary, as in the speed transient test, the detuned FLC presents the worst load rejection capability with a significant steady-state speed tracking error (around 20%). From this point of view, it can be observed a very fast torque response obtained with the MPC is associated with a higher torque ripple, which does not imply good speed dynamics for the above-cited reasons. Coherently, the i_{sx}, i_{sy} waveforms in Fig. 16 present the expected square-like shapes. As in the speed transient test, the detuned FLC presents completely

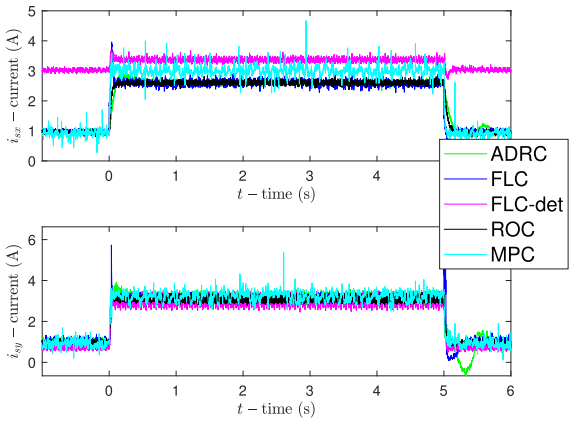

FIGURE 16. i_{sx}, i_{sy} at constant speed of 50 rad/s with 5 Nm load step torque (experiment).

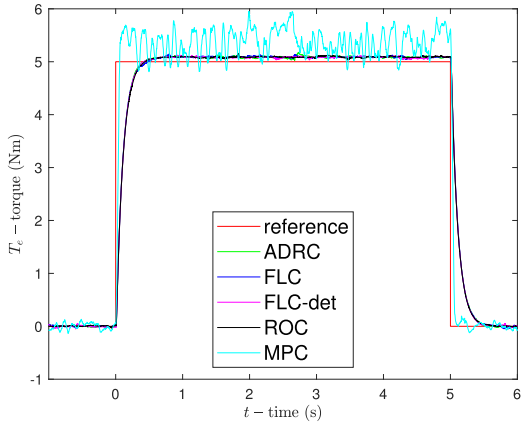

FIGURE 17. Estimated and load torques at constant speed of 50 rad/s with 5 Nm load step torque (experiment).

different steady-state values of i_{sx}, i_{sy}. Finally, the torque waveform, given in Fig. 17, shows a correct drive behavior with a very fast torque response obtained with all the controllers.

To highlight the importance of the robustness achievable with the ADRC, the reduction of the dynamic performance obtained with the FLC has been analyzed, purposely imposing an error in the knowledge of the main model parameters adopted by the controller. In particular, wrong values of the static inductances L_{sxx}, L_{syy} as well as the stator resistance R_s have been imposed to the FLC, in an operating range of ±40%. Figs. 18 and 19 show the surfaces and Fig. 20 the plot describing the IAE of the i_{sx} and speed loops versus the percent variations of L_{sxx}, L_{syy}, and R_s, computed on a speed start-up of the SynRM drive from 0 to 50 rad/s at no load; the drive has been operated under the MTPA technique in [40]; thus a contemporary variation of i_{sx} and the speed occurs. Both surfaces Figs. 18 and 19, related to the variations of L_{sxx} and L_{syy}, clearly show that the minimum value of IAE is achieved when the controller is correctly tuned, as expected. At the same time, they show that the maximum increase of the IAE, corresponding to the highest reduction of the dynamic performance, is obtained when the contemporary maximum

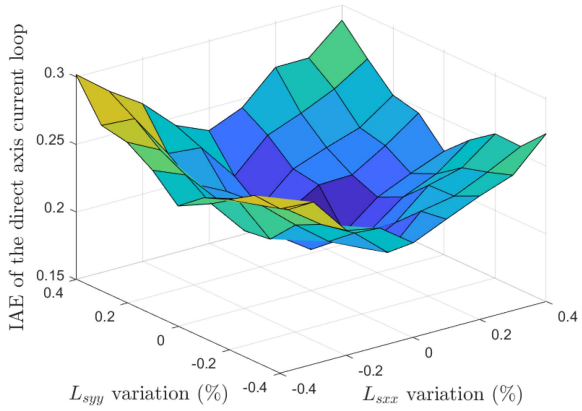

FIGURE 18. IAE of the i_{sx} loop vs the % variation of L_{sxx} and L_{syy} with FLC (experiment).

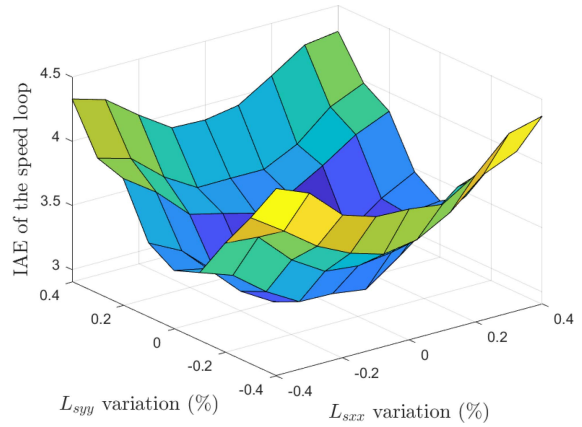

FIGURE 19. IAE of the speed loop versus the % variation of L_{sxx} and L_{syy} with *FLC* (experiment).

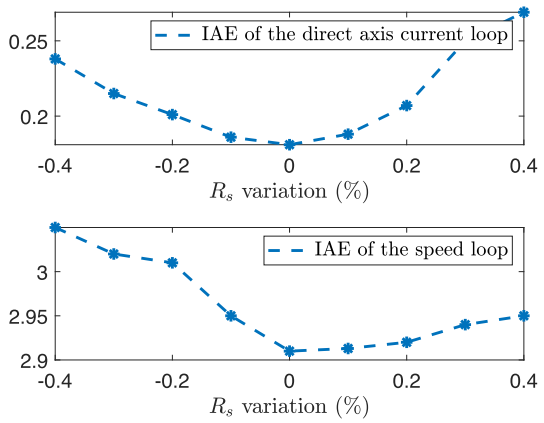

FIGURE 20. IAE of the i_{sx} and speed loops versus the % variation of R_s with *FLC* (experiment).

variations of L_{sxx} and L_{syy} occur. The noticeable maximum IAE increase is up to 40% for the i_{sx} loop and 25% for the speed loop, witnessing a significant decrease in the dynamic performance under detuned conditions. Fig. 20, related to the variation of R_s, exhibits the same kind of variation of the IAE index. Even in this case, the minimum values of the IAE indexes are obtained when the value of R_s is correctly

tuned. At the same time, the maximum increase of the IAE is observable for the highest variation of R_s, with a percent increase up to 40% in the i_{sx} loop and 20% for the speed loop. The above tests fully justify the adoption of the ADRC to improve dynamic performance with respect to the ROC case and improve the robustness of the control action in detuned working conditions.

VII. CONCLUSION

This article presents the theoretical development and the experimental application of the ADRC of SynRM. The ADRC is a particular nonlinear control technique: it can be considered as a particular kind of FLC, where the nonlinear transformation of the state is estimated online rather than computed employing the model. This approach addresses the unmodeled dynamics, uncertain model parameters, and exogenous disturbances. The effectiveness of the proposed control law has been verified experimentally on a suitably developed test setup. Experimental results fully confirm the high dynamic performance ensured theoretically by ADRC. The proposed ADRC has been experimentally compared with the classic ROC, with FLC in both tuned and detuned conditions, and with MPC. Results clearly show the advantages of adopting the ADRC in terms of dynamic performance and robustness versus model/parameters unknown.

REFERENCES

[1] L. Xu, X. Xu, T. A. Lipo, and D. W. Novotny, "Vector control of a synchronous reluctance motor including saturation and iron loss," *IEEE Trans. Ind. Appl.*, vol. 27, no. 5, pp. 977–985, Sep./Oct. 1991.

[2] R. E. Betz, R. Lagerquist, M. Jovanovic, T. J. Miller, and R. H. Middleton, "Control of synchronous reluctance machines," *IEEE Trans. Ind. Appl.*, vol. 29, no. 6, pp. 1110–1122, Nov./Dec. 1993.

[3] A. Vagati, M. Pastorelli, and G. Franceschini, "High-performance control of synchronous reluctance motors," *IEEE Trans. Ind. Appl.*, vol. 33, no. 4, pp. 983–991, Jul./Aug. 1997.

[4] I. Boldea, M. C. Paicu, and G.-D. Andreescu, "Active flux concept for motion-sensorless unified AC drives," *IEEE Trans. Power Electron.*, vol. 23, no. 5, pp. 2612–2618, Sep. 2008.

[5] R. Marino, P. Tomei, and C. M. Verrelli, *Induction Motor Control Design*. Berlin, Germany: Springer Science & Business Media, 2010.

[6] R. Marino, S. Peresada, and P. Valigi, "Adaptive input-output linearizing control of induction motors," *IEEE Trans. Autom. Control*, vol. 38, no. 2, pp. 208–221, Feb. 993.

[7] H. A. Zarchi, J. Soltani, A. Maleknia, and G. R. A. Markadeh, "A Lyapunov based nonlinear speed tracking controller for synchronous reluctance motor using adaptive input-output feedback linearization technique," in *Proc. IEEE Int. Conf. Ind. Technol.*, 2008, pp. 1–5.

[8] H. A. Zarchi, J. Soltani, and G. A. Markadeh, "Adaptive input-output feedback-linearization-based torque control of synchronous reluctance motor without mechanical sensor," *IEEE Trans. Ind. Electron.*, vol. 57, no. 1, pp. 375–384, Jan. 2010.

[9] H.-D. Lee, S.-J. Kang, and S.-K. Sul, "Efficiency-optimized direct torque control of synchronous reluctance motor using feedback linearization," *IEEE Trans. Ind. Electron.*, vol. 46, no. 1, pp. 192–198, Feb. 1999.

[10] M. Nabipour, H. A. Zarchi, and S. Madani, "Robust position control of synchronous reluctance motor drives using linear variable structure and adaptive input-output feedback linearization approaches," in *Proc. IEEE Iranian Conf. Elect. Eng.*, 2011, pp. 1–5.

[11] A. Accetta, M. Cirrincione, M. Pucci, and A. Sferlazza, "Feedback linearization based nonlinear control of SynRM drives accounting for self-and cross-saturation," *IEEE Trans. Ind. Appl.*, vol. 58, no. 3, pp. 3637–3651, May/Jun. 2022.

[12] J. Han, "From PID to active disturbance rejection control," *IEEE Trans. Ind. Electron.*, vol. 56, no. 3, pp. 900–906, Mar. 2009.

[13] Y. Huang and W. Xue, "Active disturbance rejection control: Methodology and theoretical analysis," *ISA Trans.*, vol. 53, no. 4, pp. 963–976, 2014.

[14] J. Li, Y. Xia, X. Qi, and Z. Gao, "On the necessity, scheme, and basis of the linear-nonlinear switching in active disturbance rejection control," *IEEE Trans. Ind. Electron.*, vol. 64, no. 2, pp. 1425–1435, Feb. 2017.

[15] Y. X. Su, C. H. Zheng, and B. Y. Duan, "Automatic disturbances rejection controller for precise motion control of permanent-magnet synchronous motors," *IEEE Trans. Ind. Electron.*, vol. 52, no. 3, pp. 814–823, Jun. 2005.

[16] H. Sira-Ramírez, J. Linares-Flores, C. García-Rodríguez, and M. A. Contreras-Ordaz, "On the control of the permanent magnet synchronous motor: An active disturbance rejection control approach," *IEEE Trans. Control Syst. Technol.*, vol. 22, no. 5, pp. 2056–2063, Sep. 2014.

[17] C. Liu, G. Luo, X. Duan, Z. Chen, Z. Zhang, and C. Qiu, "Adaptive LADRC-based disturbance rejection method for electromechanical servo system," *IEEE Trans. Ind. Appl.*, vol. 56, no. 1, pp. 876–889, Jan./Feb. 2020.

[18] L. Qu, W. Qiao, and L. Qu, "An enhanced linear active disturbance rejection rotor position sensorless control for permanent magnet synchronous motors," *IEEE Trans. Power Electron.*, vol. 35, no. 6, pp. 6175–6184, Jun. 2020.

[19] P. Lin, Z. Wu, K.-Z. Liu, and X.-M. Sun, "A class of linear-nonlinear switching active disturbance rejection speed and current controllers for PMSM," IEEE Trans. Power Electron., vol. 36, no. 12, pp. 14366–14382, Dec. 2021.

[20] M. Tian, B. Wang, Y. Yu, Q. Dong, and D. Xu, "Discrete-time repetitive control-based ADRC for current loop disturbances suppression of PMSM drives," *IEEE Trans. Ind. Inform.*, vol. 18, no. 5, pp. 3138–3149, May 2022.

[21] Z. Zhang, Y. Chen, X. Feng, S. Xie, and C. Zhao, "Linear active disturbance rejection speed control with variable gain load torque sliding mode observer for IPMSMs," *J. Power Electron.*, vol. 22, no. 8, pp. 1290–1301, 2022.

[22] A. M. Diab, S. S. Yeoh, S. Bozhko, C. Gerada, and M. Galea, "Enhanced active disturbance rejection current controller for permanent magnet synchronous machines operated at low sampling time ratio," *IEEE J. Emerg. Sel. Topics Ind. Electron.*, vol. 3, no. 2, pp. 230–241, Apr. 2022.

[23] Q. Hou, Y. Zuo, J. Sun, C. H. Lee, Y. Wang, and S. Ding, "Modified nonlinear active disturbance rejection control for PMSM speed regulation with frequency domain analysis," *IEEE Trans. Power Electron.*, vol. 38, no. 7, pp. 8126–8134, Jul. 2023.

[24] A. Accetta, M. Cirrincione, F. D'Ippolito, M. Pucci, and A. Sferlazza, "Adaptive feedback linearization control of SynRM drives with online inductance estimation," *IEEE Trans. Ind. Appl.*, vol. 59, no. 2, pp. 1824–1835, Mar./Apr. 2023.

[25] A. Accetta, M. Cirrincione, M. Luna, M. Pucci, and A. Sferlazza, "A model modulated predictive current control algorithm for the synchronous reluctance motor," in *Proc. IEEE Energy Convers. Congr. Expo.*, 2022, pp. 1–7.

[26] A. Accetta, M. Cirrincione, F. D'Ippolito, M. Pucci, and A. Sferlazza, "Active disturbance rejection control of synchronous reluctance motors," in *Proc. IEEE Energy Convers. Congr. Expo.*, 2020, pp. 5347–5352.

[27] M. F. Elmorshedy, W. Xu, F. F. El-Sousy, M. R. Islam, and A. A. Ahmed, "Recent achievements in model predictive control techniques for industrial motor: A comprehensive state-of-the-art," *IEEE Access*, vol. 9, pp. 58170–58191, 2021.

[28] A. Zanelli, J. Kullick, H. M. Eldeeb, G. Frison, C. M. Hackl, and M. Diehl, "Continuous control set nonlinear model predictive control of reluctance synchronous machines," *IEEE Trans. Control Syst. Technol.*, vol. 30, no. 1, pp. 130–141, Jan. 2022.

[29] T. Li, X. Sun, G. Lei, Y. Guo, Z. Yang, and J. Zhu, "Finite-control-set model predictive control of permanent magnet synchronous motor drive systems—An overview," *IEEE/CAA J. Automatica Sinica*, vol. 9, no. 12, pp. 2087–2105, Dec. 2022.

[30] X. Gao, M. Abdelrahem, C. M. Hackl, Z. Zhang, and R. Kennel, "Direct predictive speed control with a sliding manifold term for PMSM drives," *IEEE Trans. Emerg. Sel. Topics Power Electron.*, vol. 8, no. 2, pp. 1258–1267, Jun. 2020.

[31] X. Liu et al., "Continuous control set predictive speed control of SPMSM drives with short prediction horizon," IEEE Trans. Power Electron., vol. 37, no. 9, pp. 10166–10177, Sep. 2022.
[32] M. Preindl and S. Bolognani, "Model predictive direct speed control with finite control set of PMSM drive systems," *IEEE Trans. Power Electron.*, vol. 28, no. 2, pp. 1007–1015, Feb. 2013.
[33] J. Rodríguez, M. A. Pérez, H. Young, and H. Abu-Rub, "Model predictive speed control of electrical machines," *Power Electron. Renewable Energy Syst., Transp. Ind. Appl.*, pp. 608–629, 2014.
[34] S. Ding, Q. Hou, and H. Wang, "Disturbance-observer-based second-order sliding mode controller for speed control of PMSM drives," *IEEE Trans. Energy Convers.*, vol. 38, no. 1, pp. 100–110, Mar. 2023.
[35] S. Lin, Y. Cao, Z. Wang, Y. Yan, T. Shi, and C. Xia, "Speed controller design for electric drives based on decoupling two-degree-of-freedom control structure," *IEEE Trans. Power Electron.*, vol. 38, no. 12, pp. 15996–16009, Dec. 2023.
[36] Z. Li, L. Zhou, and J. Wang, "Active disturbance rejection current control for synchronous reluctance motor," in *Proc. IEEE 4th Student Conf. Electric Machines Syst.*, 2021, pp. 1–5.
[37] A. Accetta, M. Cirrincione, M. Pucci, and A. Sferlazza, "Space-vector state dynamic model of SynRM considering self-and cross-saturation and related parameter identification," *IET Electric Power Appl.*, vol. 14, no. 14, pp. 2798–2808, 2021.
[38] B.-Z. Guo and Z.-l. Zhao, "On the convergence of an extended state observer for nonlinear systems with uncertainty," *Syst. Control Lett.*, vol. 60, no. 6, pp. 420–430, 2011.
[39] H. K. Khalil, *Nonlinear Systems*. Hoboken, NJ, USA: Prentice Hall, 2002, vol. 3.
[40] A. Accetta, M. Cirrincione, M. C. Di Piazza, G. La Tona, M. Luna, and M. Pucci, "Analytical formulation of a maximum torque per ampere (MTPA) technique for SynRMs considering the magnetic saturation," *IEEE Trans. Ind. Appl.*, vol. 56, no. 4, pp. 3846–3854, Jul./Aug. 2020.

ANGELO ACCETTA (Senior Member, IEEE) received the master's degree in electrical engineering and the Ph.D. degree in electrical engineering, in collaboration with the Institute for Studies on Intelligent Systems for Automation (ISSIA) - National Research Council (CNR), University of Palermo, Palermo, Italy, in 2008 and 2011, respectively.

From 2013 to 2018, he was a Junior Researcher with the Section of Palermo, ISSIA-CNR, working to new energy management strategies for distributed generation systems and to the implementation of new sensorless control strategies for permanent magnets synchronous electric motors and for induction motors both rotating and linear. He is currently a Junior Researcher with the Institute of Marine engineering-CNR. His research interest includes sensorless control systems for electric drives with induction, rotating and linear, motors, with particular attention to their applications for electric generation systems and electric propulsion.

MAURIZIO CIRRINCIONE (Senior Member, IEEE) received the Laurea degree in electrical engineering from the Polytechnic University of Turin, Turin, Italy, in 1991, and the Ph.D. degree in electrical engineering from the University of Palermo, Palermo, Italy, in 1996.

From 1996 to 2005, he was a Researcher with the Institute on Intelligent Systems for Automation-National Research Council Section of Palermo, Palermo, Italy. In 2005, he joined the University of Technology of Belfort-Montbeliard, Belfort, France, as a Full Professor. He is currently the Head of the "School of Engineering and Physics," University of the South Pacific, Suva, Fiji. His research interests include neural networks for modeling and control, system identification, intelligent control, power electronics, renewable energy systems, and electrical machines and drives.

Dr. Cirrincione was the recipient the 1997 "E.R.Caianiello" prize for the best Italian Ph.D. thesis on neural networks.

FILIPPO D'IPPOLITO (Senior Member, IEEE) was born in Palermo, Italy, in 1966. He received the Laurea degree in electronic engineering and the Research Doctorate degree in systems and control engineering from the University of Palermo, Palermo, Italy in 1991 and 1996, respectively.

He is currently a Research Associate with the Department of Systems and Control Engineering, University of Palermo. His research interests include control of electrical drives, control of electrical power converters, adaptive and visual/force control of robot manipulators, rehabilitation robotics, and marine robotics.

Dr. D'Ippolito was the recipient of the 2000 Kelvin Premium from the Institution of Electrical Engineers, for the paper: Parameter identification of induction motor model using genetic algorithms.

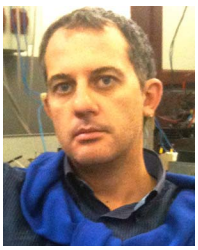

MARCELLO PUCCI (Senior Member, IEEE) received the Laurea and Ph.D. degrees in electrical engineering from the University of Palermo, Palermo, Italy, in 1997 and 2002, respectively.

In 2000, he was a Host Student with the Institute of Automatic Control, Technical University of Braunschweig, Braunschweig, Germany, working in the field of control of ac machines, with a grant from the German Academic Exchange Service. From 2001 to 2018, he has been with the Institute of Intelligent Systems for Automation, Section of Palermo, National Research Council of Italy, Rome, Italy. He is currently a Senior Researcher with the Institute of Marine Engineering-National Research Council. His research interests include electrical machines; control, diagnosis, and identification techniques of electrical drives; and intelligent control and power converters.

Dr. Pucci a Member of the Editorial Board of the Journal of Electrical Systems. He serves as an Associate Editor for IEEE TRANSACTIONS ON INDUSTRIAL ELECTRONICS and IEEE TRANSACTIONS ON INDUSTRY APPLICATIONS.

ANTONINO SFERLAZZA (Senior Member, IEEE) was born in Palermo, Italy, in 1987. He received the master's degree in automation engineering and the Ph.D. degree in mathematics and automation from the University of Palermo, Palermo, Italy, in 2011 and 2015, respectively.

In 2013, he was a Visiting Ph.D. Student with the University of California at Santa Barbara, Santa Barbara, CA, USA, in the field of modeling and analysis of stochastic hybrid systems. From 2016 to 2017, he was with the University of Palermo, as a Junior Researcher. From 2017 to 2018, he was a Researcher with LAAS CNRS, Toulouse, France, working in the field of power converter control. He is currently a systems and control engineering Researcher with the University of Palermo. His research interests include the development of feedback control algorithms for nonlinear dynamical systems, optimization techniques, estimation of stochastic dynamical systems, and applications of control of electrical drives, power converters, and mechanical systems.

Dr. Sferlazza serves as an Associate Editor for the *European Journal of Control*. He is a Technology Conferences Editorial Board member of the IEEE Control System Society.

Open Access funding provided by 'Consiglio Nazionale delle Ricerche-CARI-CARE-ITALY' within the CRUI CARE Agreement